SCIEPublish

Article

Maxillary Molar Enamel Dentine-Junction Shape Differences between Krapina Neanderthals and Modern Humans

Miguel Delgado [1,2,3,*]

[1] Anthropology Division, Faculty of Natural Sciences and Museum, National University of La Plata, La Plata B1900, Argentina
[2] National Scientific and Technical Research Council (CONICET), Buenos Aires C1425FQB, Argentina
[3] Ministry of Education Key Laboratory of Contemporary Anthropology Collaborative Innovation Center of Genetics and Development, School of Life Sciences and Human Phenome Institute Fudan University, Shanghai 200438, China

* Corresponding author. E-mail: medelgado@fcnym.unlp.edu.ar (M.D.)

Received: 27 August 2024; Accepted: 10 September 2024; Available online: 11 September 2024

ABSTRACT: Archaic and modern humans differ in a range of craniodental features. From a taxonomic and phylogenetic perspective, it is essential to distinguish between species accurately through detailed morphological characterizations. This study analyzes the size and shape variation of the enamel-dentine junction (EDJ) of upper molars from two hominin species, early Neanderthals from Krapina (N = 13) and mid-Holocene European modern humans (N = 14), to assess the extent of their endostructural morphological differentiation. The EDJ was obtained through microtomographic scans of each molar using segmentation procedures. Three-dimensional landmarks semilandmarks and 3D geometric morphometric methods, were employed to investigate EDJ size and shape variation through univariate (*t*-test), multivariate exploratory, and classification methods (PCA and LDA). The results indicate that the shape of the EDJ and cervix of M^2 differentiates Krapina Neanderthals from mid-Holocene European modern humans with a high degree of accuracy (~85%). Furthermore, EDJ size and dental nonmetric traits expressed in this structure provide additional information that is useful for distinguishing between the two species. Compared to modern humans, Krapina Neanderthals exhibit reduced dental diversity. From an endostructural perspective, this study provides additional insights into early Neanderthals' morphological diversification relative to modern humans, which is valuable for studying middle and late Pleistocene hominin evolution.

Keywords: Early Neanderthals; Modern humans; Enamel-dentine junction; Upper molars; 3D geometric morphometrics

1. Introduction

The skeletal sample from the Krapina site in Croatia, dated to about 130 ka BP [1], represents one of the largest collections of early European Neanderthals currently available for research, originating from a single site and period (MIS 5e). This collection has been systematically used in hominin evolutionary comparative studies [2–4]. However, comparisons have been hindered by the fragmentary nature of the Krapina skeletal remains. According to previous research, the Krapina Neanderthals had craniodental features similar to those of Western European Neanderthals, were differentiated from modern humans, and exhibited reduced morphological variation [2–5]. Additional investigations have provided further insights into the behaviour, skeletal trauma, health, and diet of the Neanderthal population buried at Hušnjakovo rock-shelter [6–10].

Given that teeth are better preserved than other skeletal parts, the Krapina sample consists mostly of isolated teeth (~293 teeth and tooth fragments), maxillae, and mandibles, representing the largest well-preserved sample of Neanderthal teeth found at the same site to date. Over the past decades, the dental sample from Krapina was extensively investigated, and most studies focused on the gross morphology of teeth, especially the outer enamel surface (OES) [2,4–6,11–16]. More recently, with the advent of new technologies and approaches, like microcomputed tomography and 3D geometric morphometrics, the endostructural morphology of the Krapina dental remains has been further investigated. Despite the fact that the inner morphology of Krapina teeth has been systematically used in hominin taxonomic studies, e.g., [17,18] and represents a significant portion of the total number of Neanderthal teeth currently available for study [9], few investigations have focused exclusively on the Krapina teeth to characterize the enamel-

https://doi.org/10.70322/natanthropol.2024.10017

dentine junction (EDJ) morphology and evaluate specific differences with modern humans, providing additional insights into Late Pleistocene hominin diversification and evolution.

Teeth play a significant role in the study of diversity and evolution of living and extinct hominoids [19–21]. Compared to bony elements, teeth are made of several tissues (enamel, dentine, pulp, cementum) and grow incrementally without being remodeled once they are mineralized. In addition, while both enamel and dentine are under strict genetic control in growth and development [21–26], they have different genetic backgrounds and embryogenic origins [27,28]. While enamel tends to reflect macroevolutionary changes, dentine is more conservative and records microevolutionary trajectories [28–34]. Owing to these characteristics and their better preservation and higher abundance in the fossil record, teeth are currently systematically used in paleoanthropology to reconstruct hominin evolution [35–47].

This report presents additional evidence of the size and shape differentiation between early Neanderthals from Krapina and mid-Holocene modern humans by investigating the EDJ surface of the second upper molars using 3D geometric morphometrics.

2. Materials and Methods

2.1. Materials

The sample investigated comprises 3D models of the EDJ of 27 s upper molars of two extinct and extant hominin taxa, namely early Neanderthals and modern humans. Table 1 shows details about the sample used in the present study. The Neanderthal sample consists of 13 molars from the Krapina site (dating to MIS 5e). In contrast, the modern human sample consists of 14 teeth from the archaeological site Gurgy, located in the southern Paris Basin (Yonne, France), whose radiocarbon chronology ranges from 5100 to 4000 cal BC [48]. The Krapina sample derives from the fossil virtual collection at the Stiftung Neanderthal Museum (https://archiv.neanderthal.de/) (accessed in 2023), while the modern human sample was downloaded from the open-source repository MorphoMuseum (https://morphomuseum.com/) [49] (accessed in 2021).

Table 1. Composition of the second upper molar sample included in the present study.

Site	Specimen	Taxonomy	M^2	Institution	Source	Inventory Number
Krapina	D96	Neanderthal	Right	CNHM	1, 2	F_Kra_Hn_092
	D98	Neanderthal	Right	CNHM	1, 2	F_Kra_Hn_094
	D99	Neanderthal	Right	CNHM	1, 2	F_Kra_Hn_100
	D101 *	Neanderthal	Left	CNHM	1, 2	F_Kra_Hn_097
	D109 *	Neanderthal	Right	CNHM	1, 2	F_Kra_Hn_105
	D135	Neanderthal	Left	CNHM	1, 2	F_Kra_Hn_130
	D165	Neanderthal	Right	CNHM	1, 2	F_Kra_Hn_158
	D169	Neanderthal	Right	CNHM	1, 2	F_Kra_Hn_159
	D172	Neanderthal	Right	CNHM	1, 2	F_Kra_Hn_165
	D175	Neanderthal	Left	CNHM	1, 2	F_Kra_Hn_168
	D176	Neanderthal	Left	CNHM	1, 2	F_Kra_Hn_169
	D178	Neanderthal	Right	CNHM	1, 2	F_Kra_Hn_170
	D192	Neanderthal	Left	CNHM	1, 2	F_Kra_Hn_185
Gurgy	201	Modern human	Left	UB	3	GLN04-201-ULM2
	206	Modern human	Left	UB	3	GLN04-206-ULM2
	213	Modern human	Right	UB	3	GLN05-213-URM2
	215A	Modern human	Right	UB	3	GLN05-215A-URM2
	215B	Modern human	Right	UB	3	GLN05-215B-URM2
	223	Modern human	Right	UB	3	GLN06-223-URM2
	229	Modern human	Right	UB	3	GLN04-229-URM2
	252	Modern human	Left	UB	3	GLN04-252-ULM2
	253	Modern human	Left	UB	3	GLN04-253-ULM2
	264	Modern human	Left	UB	3	GLN04-264-ULM2
	289B	Modern human	Right	UB	3	GLN04-289B-URM2
	292	Modern human	Right	UB	3	GLN05-292-URM2
	301	Modern human	Right	UB	3	GLN05-301-ULM2
	308	Modern human	Right	UB	3	GLN05-308-URM2

* Tooth reclassified as M^2 by Martin et al. [18]; CNHM—Croatian Natural History Museum; UB—University of Bordeaux; 1 = Stiftung Neanderthal Museum (2023); 2 = Nespos Database (2023); 3 = Morphomuseum Database (2021).

The upper molars investigated are well-preserved and, in all cases, suitable for the morphogeometric characterization performed. Teeth from the left side were arbitrarily chosen to represent each specimen. In such cases where only a right molar was presented, it was mirrored in Avizo Standard Edition 7.1.0 (www.vsg3d.com). Sex was unknown for several specimens and thus was not included in this analysis as a potential source of dental shape variation. Likewise, teeth with pathologies, extensive fractures, postmortem damage, and wear were excluded from this study. For the Neanderthal sample, given the uncertainty in the correct tooth position of some molars, the GM-based reclassification performed by Martin et al. [18] was used.

Microcomputed Tomography and 3D Image Processing

The dental scans were performed using different µCT systems with distinct parameters and resolutions, but in all cases, they were suitable for analysis. Microtomographic scans of M^2 for the modern human sample were obtained using a Skyscan 1076 X-ray equipment set at the MRI platform (University Montpellier 2, Montpellier, France). Acquisitions were realized according to the following parameters: 100 kV voltage, 100 µA current, a 1.0 mm aluminum filter, and a rotation step each 0.20°. The software Nrecon v1.6.6 (Skyscan) was used to reconstruct the final volumes with an isotropic voxel size ranging from 17.93 µm for isolated teeth to 36.18 µm for jaw fragments [48]. The micro-CT data for the Krapina specimens (voxel size: 20–40 µm) were obtained from NESPOS© microtomographic database housed at the Stiftung Neanderthal Museum (https://archiv.neanderthal.de/).

The modern human 3D EDJ models were derived from the MorphoMuseum site [49] and obtained using the above-mentioned parameters. For the fossil sample, TIFF image stacks were imported into Avizo Standard Edition v. 7.1.0. (www.vsg3d.com). Using the watershed tool, a semi-automatic threshold-based segmentation, with manual corrections, was performed. Accordingly, crowns and roots (when available) were digitally isolated, and the enamel and dentine tissues were segmented. Three-dimensional (3D) surface models were generated using a constrained smoothing algorithm and exported in .ply format.

2.2. Methods

A total of 114 3D landmarks were collected in Avizo 7.1.0 (www.vsg3D.com) into three distinct sets (Figure 1) following previous studies [18,31,41,47]: (1) 'EDJ_main' consists of four anatomical landmarks placed at the tips of dentine horns of each of the four primary cusps (protocone, paracone, metacone, and hypocone). 'EDJ_ridge' consists of 60 curve semilandmarks placed along the marginal ridges connecting the dentine horns, starting at the protocone dentine horn tip and continuing mesially. An additional semilandmark curve along the crista obliqua connecting the protocone and metacone dentine horn tips was included. 'CEJ_ridge' consists of 50 curve semilandmarks placed around the cementum enamel junction (CEJ), starting on the middle part of the buccal face of the crown, between the paracone and metacone, and continuing mesially. Anatomical landmarks and curve semilandmark sets were placed individually on each molar investigated.

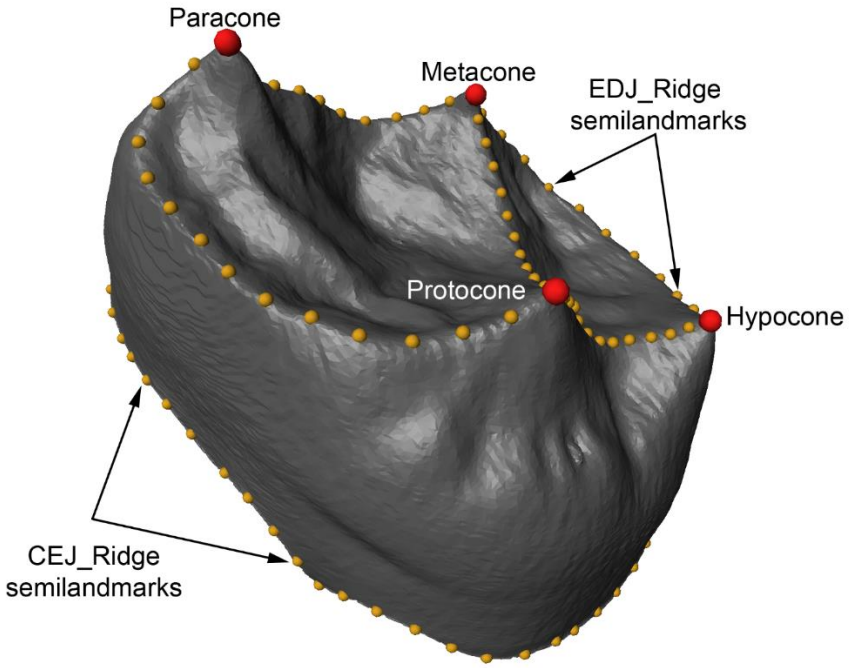

Figure 1. Landmarking protocol for the second upper molars' EDJ used in the present research. The main landmarks are highlighted in red, while the EDJ_Ridge and CEJ_Ridge semilandmarks are indicated in yellow.

The complete set of geometrically homologous landmarks for each molar was imported in R 4.1.0 software [50], using the package 'Morpho' [51]. A smooth curve was fitted to the landmarks of the EDJ_ridge and CEJ_ridge semilandmark sets, and EDJ_main landmarks were projected onto the EDJ_ridge curve, dividing it into five sections. Fifty equally spaced landmarks were placed along the CEJ_ridge semilandmarks curve, and 12 equally spaced landmarks were placed along each section of the EDJ_ridge semilandmark curve. The five sections are as follows: (1) protocone—paracone dentine horn tips, (2) paraconce—metacone dentine horn tips, (3) metacone—hypocone dentine horn tips, (4) hypocone—protocone dentine horn tips, and (5) protocone—metacone dentine horn tips. Semilandmarks were aligned along the contour of the EDJ_ridge and CEJ_ridge, sliding them along to minimize the Procrustes distance between the target and the reference using perpendicular projection or minimum Procrustes distance criteria [52]. Original configurations were superimposed using the Generalized Procrustes Analysis (GPA) to remove the effects of translation, rotation, and scaling [53]. After superimposition, the shape was condensed in the aligned specimens, and molar size was expressed as the centroid size (CS), the square root of the sum of squared distances of all landmarks of a molar EDJ from their center of gravity [54]. After this procedure, the differences observed among landmark configurations were only due to shape. From the superimposed configuration, the mean shape of individuals was obtained (the consensus shape configuration) and was used as a reference. The shape of each individual was defined by Procrustes residuals, which are the deviations of landmarks relative to the consensus [53].

Using the packages 'ade4' v.1.7-6 [55] and 'Morpho' v.2.8 [51] for R principal component analysis (PCA), and cross-validated linear discriminant analysis (LDA) were computed. The shape changes and their intensity associated with the positive and negative extremes (i.e., maximal and minimal, respectively) of the first three axes were computed in 'Morpho' using the functions 'pcaplot3d' and 'tps3d'. Distances between positive and negative PC-based shape change were calculated and visualized as heatmaps using the function 'meshDist' of the 'Morpho' package. In addition to the quantitative analyses of the shape changes, following Skinner et al. [31], a qualitative assessment was performed by comparing the mean EDJ shape of the Neanderthal and modern human samples. Using the 'Morpho' [51] and 'geomorph' [56] packages, the specimen most similar to the average of each taxan was identified. Subsequently, a 3D mean mesh was computed using the surface of the target specimen and its landmarks and the mean shape was used as a reference. Finally, the mean shape of both Neanderthals and modern humans were exported as .ply files using the 'rgl' package [57] and derived in Avizo 7.1.0 (www.vsg3D.com), to be aligned and superimposed automatically to inspect visually their morphological differentiation. An independent Student *t*-test was used to evaluate the logCS differences (the natural logarithm of centroid size) between the taxa investigated and violin plots were computed to graphically describe the variation of logCS using the package ggplot2 v3.4.1 [58].

3. Results

The results of the PCA investigating the EDJ/CEJ M^2 shape differences between early Neanderthals (green) and mid-Holocene European modern humans (yellow) are presented in Figure 2. The 3D scatterplot of the first three PCs reveals little overlap between the two taxa, as shown by the convex hulls. Despite modern humans belonging to the same archaeological site and period, they exhibit considerably more shape variation. Neanderthals show reduced diversity, but some within-group differences are evident. Along PC1 (33% of the total variance), modern humans are placed along negative values, while Neanderthals tend to be located toward the positive morphospace. PC2 (17.1% of the total variance) shows some overlap. Still, it differentiates the two taxa, with modern humans scattered along the positive and negative space and Neanderthals placed in the positive shape space. PC3 (12.5% of the total variance), despite presenting greater overlap, shows that most modern humans occupy the negative space, while most Neanderthals tend to be located in the positive shape space.

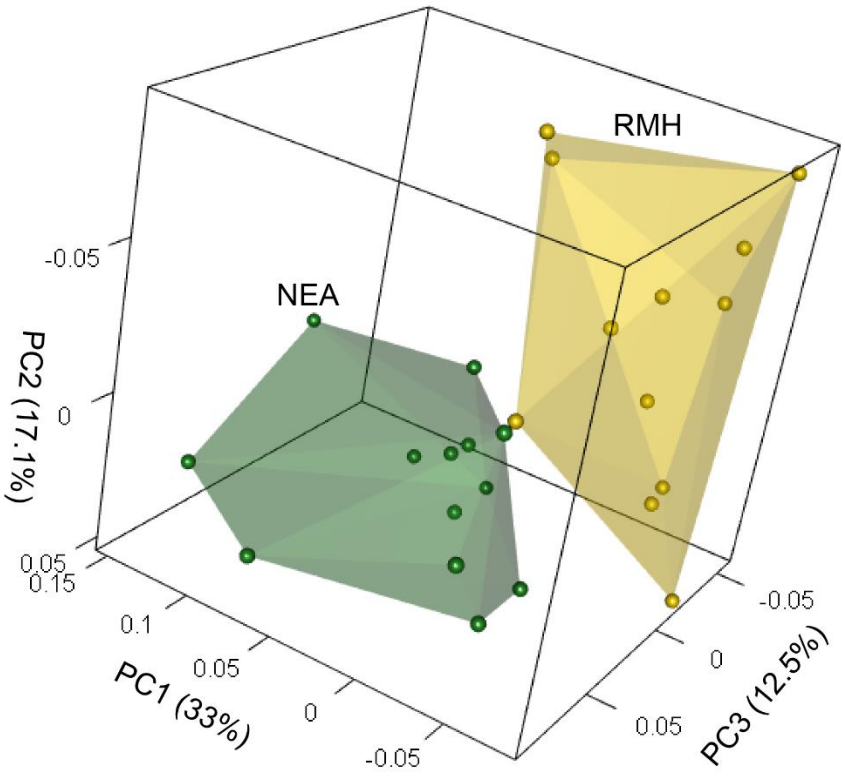

Figure 2. 3D PCA plot of the EDJ/CEJ shape of second upper molars. RMH = recent modern humans; NEA = Krapina Neanderthals.

Figures 3–5 present the shape changes associated with the first three PCs, maximal and minimal. The PC1 positive shape changes (Figure 3), viewed as displacement heatmaps from different views (occlusal, mesial, distal, buccal and lingual), reveal that the morphological M^2 EDJ differences between Neanderthals and modern humans are broadly distributed and moderate. Warm colors indicating expansions show that Neanderthals have expanded mesiobuccal and distolingual corners of the CEJ. Likewise, Neanderthals present a relatively contracted EDJ basin, including relatively wide dentine horns (i.e., paracone, metacone and hypocone), a well-developed crista obliqua (type II according to Martin et al. [18]), relatively wide EDJ mesial and distal ridges, and a more internally tilted protocone dentine horn. The PC1 negative shape changes (Figure 3) show the opposite pattern in modern humans: contraction, as indicated by the cold colors of the mesiobuccal and distolingual CEJ corners, and a remarkably reduced hypocone. Expansions are also evident in the buccal (i.e., paracone dentine horn) and lingual (i.e., protocone dentine horn) portions of the EDJ, with the protocone dentine horn being mesially contracted. PC2 positive shape changes characterizing Neanderthals (Figure 4) show expansions (warm colors) in the trigon and along the crista obliqua andin the protocone and paracone dentine horns. In addition, contractions (cold colors) are evident in the mesiobuccal corner of the CEJ, the metacone dentine horn, and the lingual and distolingual sides of the CEJ and EDJ, respectively. The PC2 negative shape changes (Figure 4) show that modern humans exhibit a remarkably contracted crista obliqua and a relatively wide talon. Expansions also charcterize the CEJ mesiobuccal corner, the metacone dentine horn and the CEJ lingual ridge. Finally, the PC3 shape changes show that Neanderthals (Figure 5) exhibit contracted metacone and hypocone dentine horns,

with expansions in the mesial ridge and in the distobuccal portion of the EDJ. Conversely, modern humans (Figure 5) display wide metacone and hypocone dentine horns, contracted mesial ridges, and a relatively expanded distolingual portion of the EDJ.

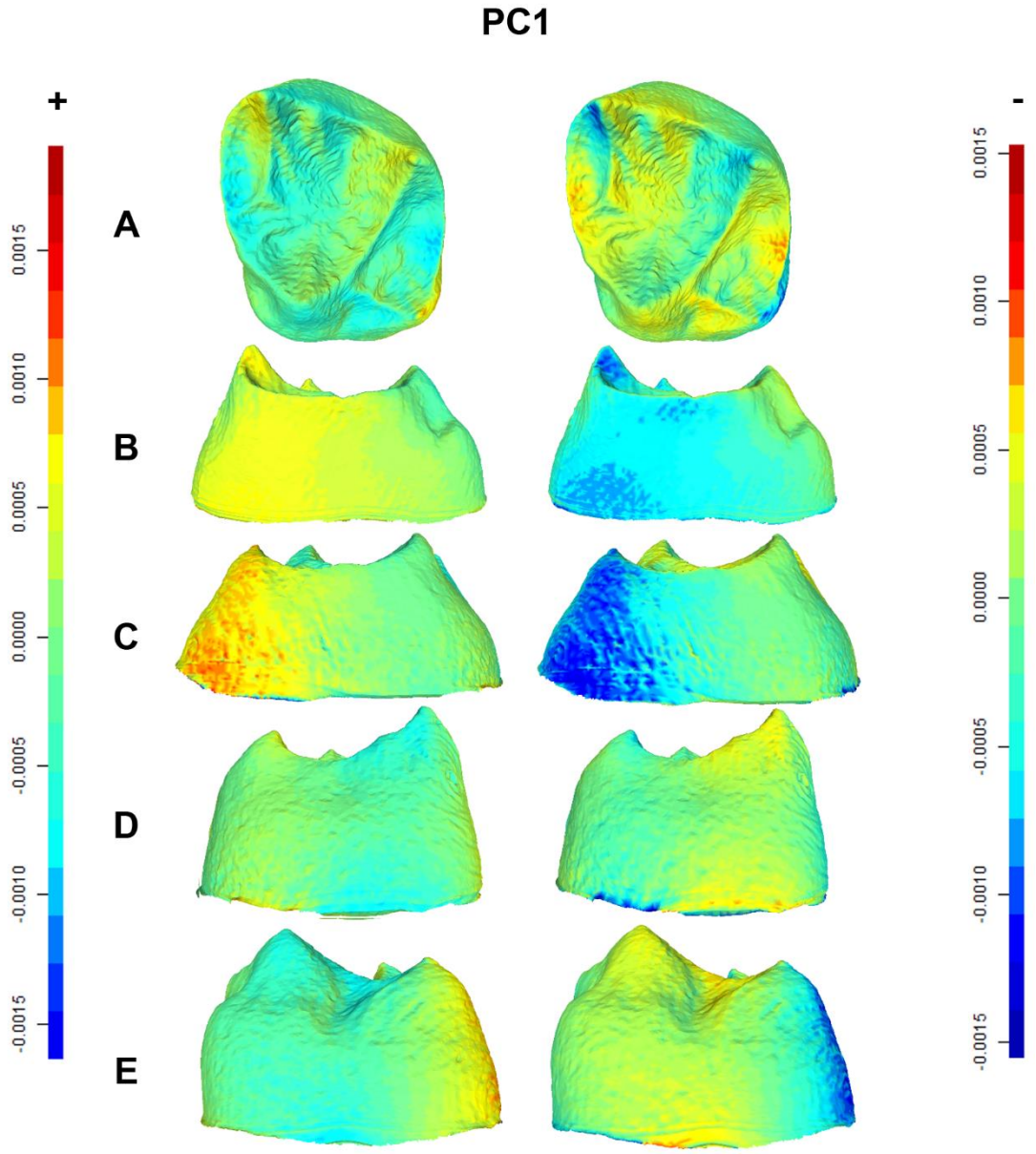

Figure 3. Displacement heatmaps associated with each extreme (positive and negative) of the PC1 for Neanderthal and modern human M^2 EDJ mean shapes, showing occlusal (**A**), mesial (**B**), distal (**C**), buccal (**D**), and lingual (**E**) views of the EDJ. Warm (red) and cold (blue) colors represent the distribution of expansion and contraction, respectively, in Procrustes shape distance. Regions of the Neanderthal mean shape outside the modern human mean shape are colored red, whereas any parts inside the modern human mean shape are colored blue. The scale bar denotes displacement in millimetres.

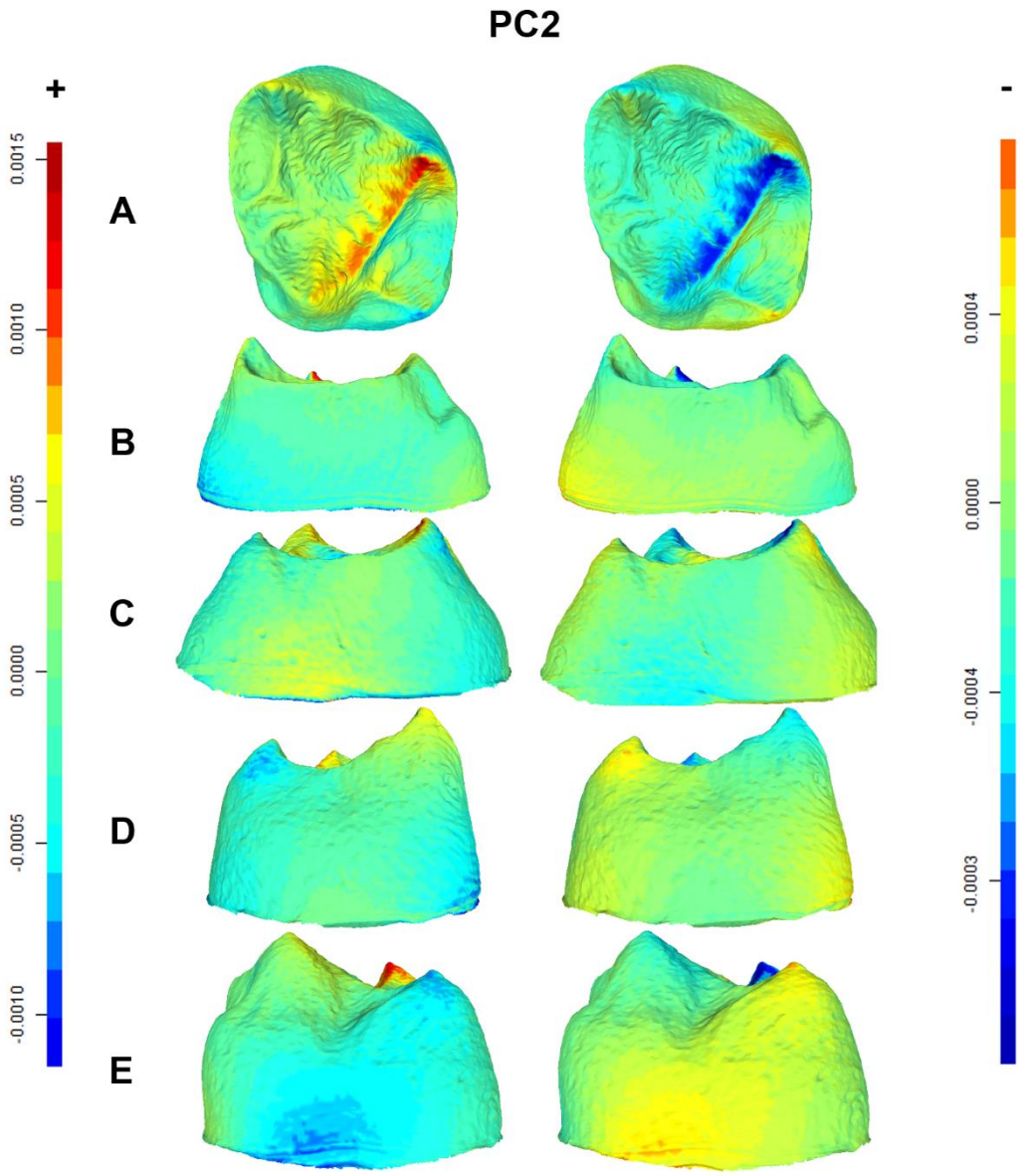

Figure 4. Displacement heatmaps associated with each extreme (positive and negative) of the PC2 for Neanderthal and modern human M^2 EDJ mean shapes, showing occlusal (**A**), mesial (**B**), distal (**C**), buccal (**D**), and lingual (**E**) views of the EDJ. Warm (red) and cold (blue) colors represent the distribution of expansion and contraction, respectively, in Procrustes shape distance. Regions of the Neanderthal mean shape outside the modern human mean shape are colored red, whereas any parts inside the modern human mean shape are colored blue. The scale bar denotes displacement in millimetres.

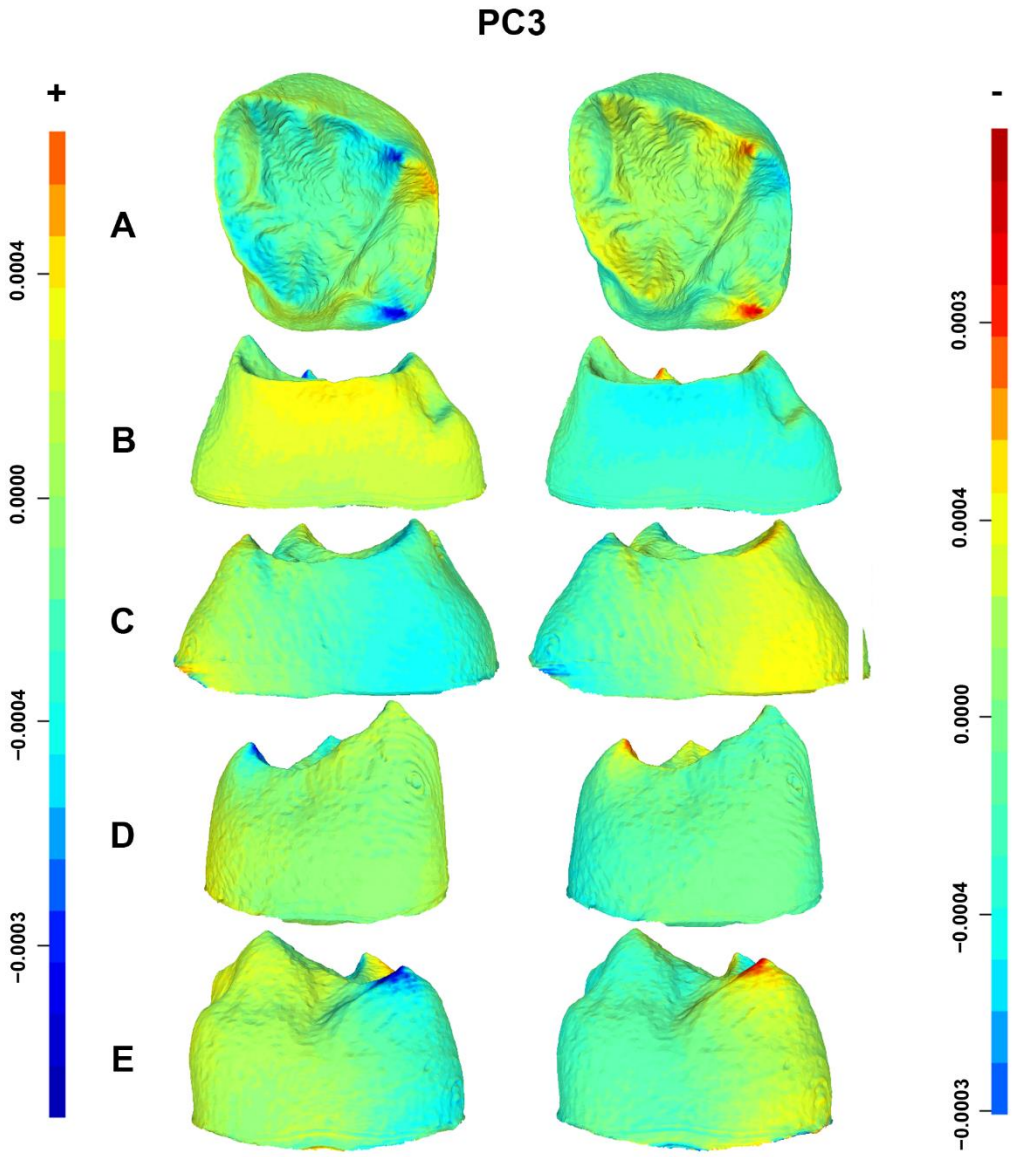

Figure 5. Displacement heatmaps associated with each extreme (positive and negative) of the PC3 for Neanderthal and modern human M^2 EDJ mean shapes, showing occlusal (**A**), mesial (**B**), distal (**C**), buccal (**D**), and lingual (**E**) views of the EDJ. Warm (red) and cold (blue) colors represent the distribution of expansion and contraction in Procrustes shape distance. Regions of the Neanderthal mean shape outside the modern human mean shape are colored red, whereas any parts inside the modern human mean shape are colored blue. The scale bar denotes displacement in millimetres.

The cross-validation classification results derived from the LDA are presented in Table 2. According to these results, both the overall classification accuracy (85%) and the kappa statistic (0.7) indicate that the M^2's EDJ and CEJ shape variation can effectively discriminate between both hominin species with high accuracy. Interestingly, modern humans were classified with 100% accuracy, while three Krapina Neanderthals were erroneously classified as modern humans. An inspection of such individuals revealed that all have a markedly reduced hypocone dentine horn, indicating that the hypocone is relevant in taxonomic discrimination. These results suggest that the EDJ ridge and cervix shape preserve a strong taxonomic signal.

Table 2. Cross-validated classification results in frequencies.

Species	Modern Humans	Neanderthals
Modern Humans	14	0
Neanderthals	3	10
Kappa statistic: 0.7 Overall classification accuracy: 85%		

In Figure 6, the comparison of the mean EDJ/CEJ shape of M^2 between Neanderthals (red) and modern humans (light blue) in different views (occlusal, mesial, distal, buccal and lingual) is presented. Neanderthals show slightly taller dentine horns, especially those corresponding to the protocone and paracone, and a taller and larger EDJ. Likewise, the trigon and talon basins are deeper in Neanderthals. In modern humans, the EDJ ridge is high and well-developed, and the buccal side of the EDJ and CEJ is projected, while in Neanderthals, it is retracted. The protocone-metacone and paracone-hypocone dentine horns are more separated in Krapina Neanderthals than in recent modern humans. The CEJ of Neanderthals is relatively larger and is buccolingually longer relative to that of mid-Holocene modern humans. The hypocone is relatively short in modern humans and Neanderthals compared to the protocone, paracone and metacone. The cervix is more rectangular in Neanderthals, while in modern humans, it is relatively circular. Finally, in the mean M^2 EDJ shape of Neanderthals and modern humans, it was possible to observe some nonmetric traits previously defined [18,59]. For instance, unlike modern humans, Neanderthals presented internally tilted dentine horn tips, especially the metacone. Likewise, despite the post-paraconce tubercle being present in both species, Neanderthals exhibited a stronger degree of expression, intermediate, according to Martin et al. [18]. Neanderthals presented a well-developed and deeper crista obliqua relative to modern humans, but both presented type II. The mesiolingual portion of the EDJ is mesially projected in Neanderthals and retracted in modern humans, and the grooves and pits indicating the presence of the Carabelli tubercle are strongly expressed in Neanderthals. Despite these shape differences being small in scale and derived from the mean shape, they reveal additional taxonomic information useful to discriminate between the two species at the EDJ and cervix levels.

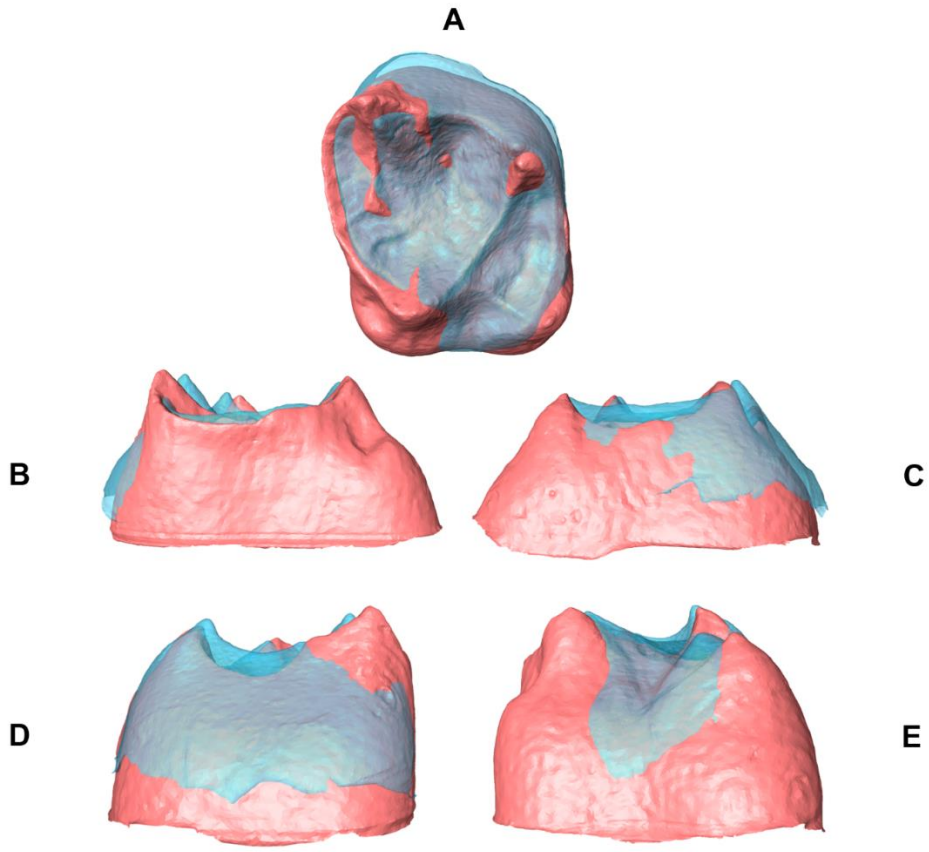

Figure 6. Comparison of the mean EDJ shape (M^2) between Neanderthals (red) and modern humans (light blue) in occlusal (**A**), mesial (**B**), distal (**C**), buccal (**D**), and lingual (**E**) views of the EDJ.

A violin plot showing the natural logarithm of M^2 centroid size in Krapina Neanderthals and European Mid-Holocene modern humans is presented in Figure 7. Neanderthal M^2 EDJ's are significantly larger than those from modern humans. Just one modern human individual has a molar size similar to that found among Neanderthals, but it falls toward the lower end of the Neanderthal range of variation. The highly significant *p*-value (1.3622×10^{-6}) suggests remarkable upper molar size differences between both species.

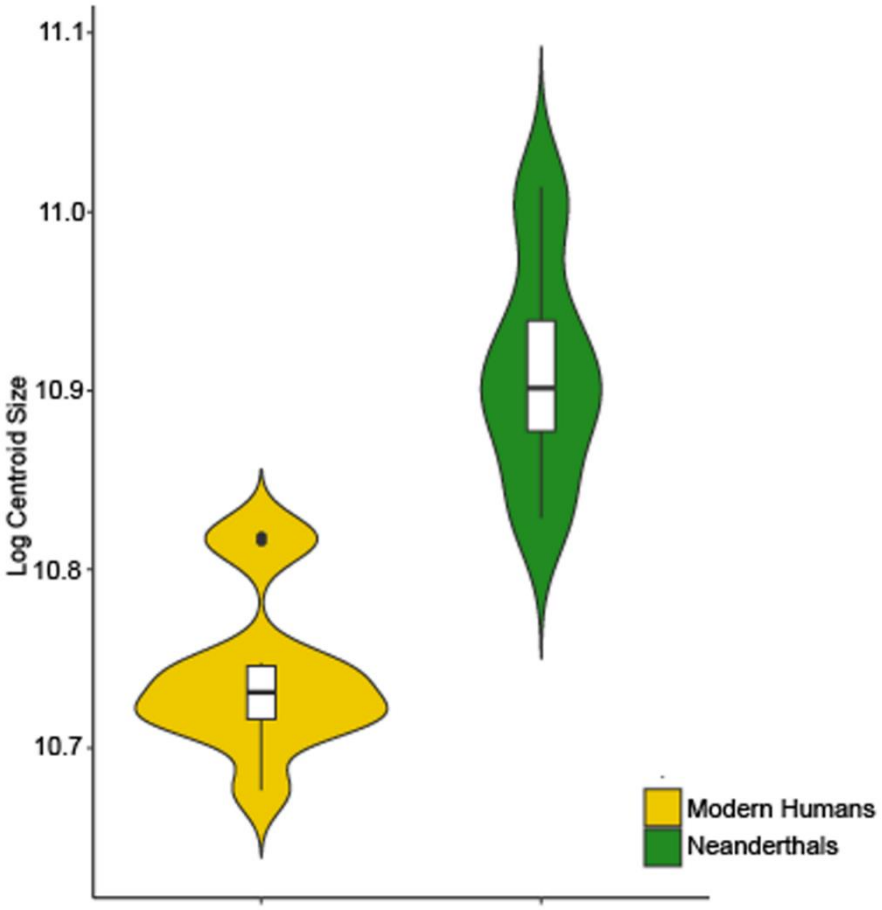

Figure 7. Violin plot of the natural logarithm of centroid size showing differences between Neanderthals (green) and modern humans (yellow).

4. Discussion

Previous taxonomic assessments at the OES level have yielded contradictory conclusions regarding the degree of morphological differentiation between Neanderthals and recent modern humans. While most quantitative analyses of the tooth shape variation at distinct tooth positions can effectively discriminate between the two species [13,14,60–62], other investigations do not find a clear morphological distinction between them [15]. Likewise, dental nonmetric trait variation patterns have revealed consistently remarkable differences, including a distinctive derived dental morphology among Neanderthals [4,12,63]. Results of the present study reveal that the EDJ/CEJ shape of upper molars retain a robust taxonomic signal that helps distinguish Krapina Neanderthals from mid-Holocene European modern humans. Previous studies that investigated the OES [15,64], but especially those that analysed upper molar endostructural morphology, are highly consistent with these results [14,18,62,65,66]. Despite Gómez-Robles et al. [15] finding that the shape of M^2 and M^3 do not differentiate well among living and fossil hominins (but see Gómez-Robles et al. [61] for a contrary result regarding M^1), they detected a pattern of distribution along the morphospace that coincides with the degree of hypocone reduction, with modern humans exhibiting higher degrees of reduction than Neanderthals. This trend was also observed in enamel thickness maps when comparing European fossil hominins [64]. This study detected a similar reduction in the hypocone dentine horn that differentiates early Neanderthals from modern humans, which is consistent with the pattern observed at the OES level. Olejniczak et al. [32] studied enamel thickness and found that hypocone reduction was associated with inflated relative enamel thickness values in modern humans at distinct tooth positions. In contrast, Neanderthals exhibited the opposite pattern, i.e., non-reduced hypocone dentine horns, thinner enamel (an alleged derived condition) and greater EDJ lengths. The results presented here align with those obtained by Benazzi et al. [14] concerning the taxonomic discrimination achieved through the cervical shape, which played a significant role in the observed difference between modern humans and early Neanderthals.

Other studies reporting isolated findings of second upper molars reinforce the degree of Neanderthal—modern human diversification viewed at the EDJ level. For example, Benazzi et al. [65] and Zubova et al. [66] reported M^2's from Southern Europe and Eurasia, respectively, with specific characteristics that defined the Neanderthal EDJ

morphology, such as a well-developed crista obliqua, a non-reduced hypocone dentine horn and distal ridge, the expression of post-paracone tubercles, and thinner enamel thickness along with internally tilted dentine horn tips in the case of the Russian Neanderthal [66], and a relatively small occlusal polygon area in the case of the Italian Neanderthal [65].

The results presented here are consistent with those obtained by Martin et al. [18], which represents the most comprehensive assessment to date of Neanderthal and modern human EDJ molar shape variation. Some differences are likely related to Martin and colleagues investigating a larger Neanderthal and recent human sample. For instance, despite detecting some overlap, as viewed from the convex hulls, M^2's differentiate Neanderthals from modern humans with accuracy values similar to or higher than those in the present investigation (Table 2, ~85%). Importantly, both studies detected lower diversity in Neanderthals than modern humans, as viewed from the EDJ, supporting previous research indicating that the Neanderthal lineage in general and the Krapina population in particular exhibited low biological diversity [5]. The EDJ/CEJ shape changes maps (Figures 3–5) and the superposition of the Neanderthal and mid-Holocene modern human EDJ mean shapes (Figure 6) show similar shape changes to those observed by Martin and colleagues [18], highlighting in Neanderthals larger EDJ's, expanded mesiobuccal and distolingual corners of the CEJ, a relatively squared cervix, more internally tilted dentine horn tips, a non-reduced hypocone, and more separated protocone-metacone and paracone-hypocone dentine horns. Mid-Holocene modern humans show the opposite pattern, including smaller EDJ's, a contracted mesiobuccal corner of the CEJ, highly reduced hypocone dentine horns and less-separated protocone-metacone and paracone-hypocone dentine horns. Some of these results also coincide with findings investigating the outer enamel surface, highlighting centrally placed cusps and a less pronounced distolingual extension of the CEJ distolingual corner in Neanderthals [13,15].

As shown above, the average EDJ shape exhibited nonmetric traits that help distinguish Neanderthals from modern humans, aligning with previous assessments [18,59]. Krapina Neanderthals presented internally tilted dentine horn tips, strongly expressed post-paraconce tubercles, a well-developed and deeper crista obliqua, strong expression of ridges, grooves and pits indicating the presence of the Carabelli tubercle at the mesiolingual portion of the EDJ, as well as expanded and deeper trigon and talon basins. Although there are multiple scoring systems available for most nonmetric features that are visible at the EDJ in different teeth and tooth positions [17,18,31,58,59,67–69], there is currently no unified system similar to those existing for dental traits expressed at the OES [70,71]. Given the differences between enamel and dentine regarding their genetic background, embryonic origins, and evolutionary trajectories, it would be necessary to establish reliable, standardized and unified protocols to score dental traits at the EDJ for use in hominoid systematics. The traits detected here and elsewhere [18,59] would be important in living and fossil hominin alpha taxonomy and phylogenetics. Their examination can contribute to elucidating previously undetected diversity between and within species and help differentiate between developmentally homologous and homoplastic features crucial in phylogenetic analyses [59,72]. As Martin et al. [18] pointed out, examining traits at the EDJ level can clarify the presence and degree of expression of certain traits useful in taxonomic assessments.

Neanderthal M^2 EDJ's are significantly larger than those from recent modern humans. This indicates, in agreement with previous studies at the OES and EDJ level [2,16,18], that molar size differentiates well between early Neanderthals and recent modern humans. However, previous studies showed that when early Neanderthals, fossil *H. sapiens*, and other middle to late Pleistocene hominins are compared, the differences became less clear, indicating that "molar size" is an unreliable proxy for taxonomic discrimination [73]. Larger EDJ's in Neanderthals are associated with thin enamel, while smaller EDJ's in modern humans are associated with thick enamel [32]. Although the causes of the differences between Neanderthals and modern humans in tooth size and dental tissue proportions (e.g., enamel thickness, EDJ surface area, coronal dentine volume and area, coronal pulp chamber, etc.) remain unclear and are ultimately related to differences in development trajectories, life history, dental tissue structural organization, dietary adaptations, body size, etc., previous analyses suggest that much of the difference in dental tissue proportions among Neanderthals and modern humans is primarily related to a greater dentine volume and area in Neanderthals [32,64,74]. In contrast, modern humans have recently experienced a remarkable dental size reduction related to a disproportionate decrease in coronal dentine [74]. The findings presented here validate the notion that some of the tooth size differences observed between Neanderthals and modern humans are associated with a larger dentine size in Neanderthals.

Finally, despite the present study not evaluating differences between early and late Neanderthals, the endostructural characterization of Krapina Neanderthals strongly supports studies that found nearly the same set of morphological features characterizing early Neanderthals [18], which, in turn, differ from late Neanderthals, supporting evolutionary models suggesting high to mean evolutionary rates and a relatively strong dental divergence in Neanderthals *sensu lato* [75]. The observed EDJ and cervix shape differences between Pre-Eemian/Eemian and Post-Eemeian Neanderthals [18]

indicate a scenario of relatively fast dental evolution in Neanderthals, influenced by both genetic drift and directional evolutionary factors [17,75].

5. Conclusions

The results presented here reinforce studies that found early Neanderthals and recent modern humans differ significantly in their upper molar endostructural morphological configurations. A series of size, shape and nonmetric features—such as larger EDJ's, wide and internally tilted dentine horns, wide and deeper trigon and talon basins, an expanded CEJ mesiobuccal corner, a relatively rectangular cervix, non-reduced hypocone dentine horns, a well-developed crista obliqua, and strongly expressed post-paracone tubercles—characterizing early Neanderthals, are useful to taxonomically differentiate them from other hominins, in this case, mid-Holocene European modern humans. Further analyses of dental morphological changes at the EDJ level from different teeth and tooth positions in Krapina Neanderthals would provide additional information useful in taxonomic and phylogenetic studies investigating Middle and Late Pleistocene hominin evolution and diversification.

Acknowledgments

The author is grateful to the Stiftung Neanderthal Museum (https://archiv.neanderthal.de/) and the open-source repository MorphoMuseum (https://morphomuseum.com/) for guaranteeing access to the materials used in this research. I want to thank Richard Scott (Department of Anthropology, University of Nevada, Reno, USA) and Pianpian Wei (Institute of Archaeological Science, Fudan University, China) for providing valuable comments and criticism to earlier versions of this manuscript. This manuscript was enriched by previous discussions with Clément Zanolli (Univ. Bordeaux, CNRS, MCC, PACEA, France) and Matt Skinner (Department of Human Origins, Max Planck Institute for Evolutionary Anthropology, Germany) about the endostructural morphological diversity of hominin teeth. I want to thank the two anonymous reviewers for their careful reading of this manuscript, constructive comments, and positive criticism.

Ethics Statement

Not applicable.

Informed Consent Statement

Not applicable.

Funding

Work leading to this publication was partially funded by grants from the National Natural Science Foundation of China (#31771393 to Andrés Ruiz-Linares) and from Wenner-Gren Foundation for Anthropological, Research Grant/Award number 9391.

Declaration of Competing Interest

The author declares that he has no known competing financial interests or personal relationships that could have appeared to influence the work reported in this paper.

References

1. Rink WJ, Schwarcz HP, Smith FH, Radovĉiĉ J. ESR ages for Krapina hominids. *Nature* **1995**, *378*, 24.
2. Wolpoff MH. The Krapina dental remains. *Am. J. Phys. Anthropol.* **1979**, *50*, 67–113.
3. Balzeau A. Variation and Characteristics of the Cranial Vault Thickness in the Krapina and Western European Neandertals. *Period. Biol.* **2007**, *109*, 369.
4. Stringer CB, Humphrey LT, Compton T. Cladistic analysis of dental traits in recent humans using a fossil outgroup. *J. Hum. Evol.* **1997**, *32*, 389–402.
5. Palancar CA, García-Martínez D, Radovčić D, Llidó S, Mata-Escolano F, Bastir M, et al. Krapina atlases suggest a high prevalence of anatomical variations in the first cervical vertebra of Neanderthals. *J. Anat.* **2020**, *237*, 579–586.
6. Frayer DW, Russell MD. Artificial grooves on the Krapina Neanderthal teeth. *Am. J. Phys. Anthropol.* **1987**, *74*, 393–405.
7. Guatelli-Steinberg D, Stinespring-Harris A, Reid DJ, Larsen CS, Hutchinson DL, Smith TM. Chronology of Linear Enamel Hypoplasia Formation in the Krapina Neanderthals. *PaleoAnthropology* **2014**, *2014*, 431–445.

8. Fiore I, Bondioli L, Frayer DW. Handedness in the Krapina Neandertals: A Re-Evaluation. *PaleoAnthropology* **2015**, *2015*, 19–36.
9. Belcastro MG, Mariotti V, Riga A, Bonfiglioli B, Frayer DW. Tooth fractures in the Krapina Neandertals. *J. Hum. Evol.* **2018**, *123*, 96–108.
10. Fiorenza L, Habashi W, Moggi-Cecchi J, Benazzi S, Sarig R. Relationship between interproximal and occlusal wear in Australopithecus africanus and Neanderthal molars. *J. Hum. Evol.* **2023**, *183*, 103423.
11. Radovčić J, Smith FH, Trinkaus E, Wolpoff MH. *The Krapina Hominids: An Illustrated Catalog of the Skeletal Collection*; Mladost and the Croatian Natural History Museum: Zagreb, Croatia, 1988.
12. Bailey SE. A closer look at Neanderthal postcanine dental morphology: The mandibular dentition. *Anat. Rec.* **2002**, *269*, 148–156.
13. Bailey SE. A morphometric analysis of maxillary molar crowns of Middle-Late Pleistocene hominins. *J. Hum. Evol.* **2004**, *47*, 183–198.
14. Benazzi S, Coquerelle M, Fiorenza L, Bookstein F, Katina S, Kullmer O. Comparison of dental measurement systems for taxonomic assignment of first molars. *Am. J. Phys. Anthropol.* **2011**, *144*, 342–354.
15. Gómez-Robles A, Bermúdez de Castro JM, Martinón-Torres M, Prado-Simón L, Arsuaga JL. A geometric morphometric analysis of hominin upper second and third molars, with particular emphasis on European Pleistocene populations. *J. Hum. Evol.* **2012**, *63*, 512–526.
16. Brace CL. Krapina, "Classic" Neanderthals, and the evolution of the European face. *J. Hum. Evol.* **1979**, *8*, 527–550.
17. Bailey SE, Skinner MM, Hublin J-J. What lies beneath? An evaluation of lower molar trigonid crest patterns based on both dentine and enamel expression. *Am. J. Phys. Anthropol.* **2011**, *145*, 505–518.
18. Martin RMG, Hublin J-J, Gunz P, Skinner MM. The morphology of the enamel–dentine junction in Neanderthal molars: Gross morphology, non-metric traits, and temporal trends. *J. Hum. Evol.* **2017**, *103*, 20–44.
19. Swindler DR. *Primate Dentition: An Introduction to the Teeth of Non-Human Primates*; Cambridge University Press: Cambridge, UK, 2002. doi:10.1017/CBO9780511542541.
20. Guatelli-Steinberg D. *What Teeth Reveal about Human Evolution*; Cambridge University Press: Cambridge, UK, 2016. doi:10.1017/CBO9781139979597.
21. Scott GR, Turner CG II, Townsend GC, Martinón-Torres M. *The Anthropology of Modern Human Teeth: Dental Morphology and Its Variation in Recent and Fossil Homo Sapiens*; Cambridge University Press: Cambridge, UK, 2018. doi:10.1017/9781316795859.
22. Kimura R, Yamaguchi T, Takeda M, Kondo O, Toma T, Haneji K, et al. A Common Variation in EDAR Is a Genetic Determinant of Shovel-Shaped Incisors. *Am. J. Hum. Genet.* **2009**, *85*, 528–535.
23. Park JH, Yamaguchi T, Watanabe C, Kawaguchi A, Haneji K, Takeda M, et al. Effects of an Asian-specific nonsynonymous EDAR variant on multiple dental traits. *J. Hum. Genet.* **2012**, *57*, 508–514.
24. Kimura R, Watanabe C, Kawaguchi A, Kim YI, Park SB, Maki K, et al. Common polymorphisms in WNT10A affect tooth morphology as well as hair shape. *Hum. Mol. Genet.* **2015**, *24*, 2673–2680.
25. Delgado M, Ramírez LM, Adhikari K, Fuentes-Guajardo M, Zanolli C, Gonzalez-José R, et al. Variation in dental morphology and inference of continental ancestry in admixed Latin Americans. *Am. J. Phys. Anthropol.* **2019**, *168*, 438–447.
26. Yang G, Chen Y, Li Q, Benítez D, Ramírez LM, Fuentes-Guajardo M, et al. Dental size variation in admixed Latin Americans: Effects of age, sex and genomic ancestry. *PLoS ONE* **2023**, *18*, e0285264.
27. Jernvall J, Thesleff I. Tooth shape formation and tooth renewal: Evolving with the same signals. *Development* **2012**, *139*, 3487–3497.
28. Morita W, Morimoto N, Kono RT, Suwa G. Metameric variation of upper molars in hominoids and its implications for the diversification of molar morphogenesis. *J. Hum. Evol.* **2020**, *138*, 102706.
29. Kraus BS. Morphologic Relationships Between Enamel and Dentin Surfaces of Lower First Molar Teeth. *J. Dent. Res.* **1952**, *31*, 248–256.
30. Korenhof C. The enamel-dentine border : A new morphological factor in the study of the (human) molar pattern. *Proc. Koninkl. Nederl. Acad. Wetensch.* **1961**, *64*, 639–664.
31. Skinner MM, Gunz P, Wood BA, Hublin J-J. Enamel-dentine junction (EDJ) morphology distinguishes the lower molars of Australopithecus africanus and Paranthropus robustus. *J. Hum. Evol.* **2008**, *55*, 979–988.
32. Olejniczak AJ, Smith TM, Feeney RN, Macchiarelli R, Mazurier A, Bondioli L, et al. Dental tissue proportions and enamel thickness in Neandertal and modern human molars. *J. Hum. Evol.* **2008**, *55*, 12–23.
33. Macchiarelli R, Bayle P, Bondioli L, Mazurier A, Zanolli C. From outer to inner structural morphology in dental anthropology: Integration of the third dimension in the visualization and quantitative analysis of fossil remains. In *Anthropological Perspectives on Tooth Morphology: Genetics, Evolution, Variation*; Scott GR, Irish JD, Eds.; Cambridge University Press: Cambridge, UK, 2013; pp. 250–277. doi:10.1017/CBO9780511984464.011.
34. Monson TA, Fecker D, Scherrer M. Neutral evolution of human enamel–dentine junction morphology. *Proc. Natl. Acad. Sci. USA* **2020**, *117*, 26183–26189.

35. Xing S, Martinón-Torres M, Bermúdez de Castro JM, Zhang Y, Fan X, Zheng L, et al. Middle Pleistocene Hominin Teeth from Longtan Cave, Hexian, China. *PLoS ONE* **2014**, *9*, e114265.
36. Smith TM, Tafforeau P, Le Cabec A, Bonnin A, Houssaye A, Pouech J, et al. Dental Ontogeny in Pliocene and Early Pleistocene Hominins. *PLoS ONE* **2015**, *10*, e0118118.
37. Fornai C, Bookstein FL, Weber GW. Variability of Australopithecus second maxillary molars from Sterkfontein Member 4. *J. Hum. Evol.* **2015**, *85*, 181–192.
38. Hlusko LJ, Schmitt CA, Monson TA, Brasil MF, Mahaney MC. The integration of quantitative genetics, paleontology, and neontology reveals genetic underpinnings of primate dental evolution. *Proc. Natl. Acad. Sci. USA* **2016**, *113*, 9262–9267.
39. Xing S, Martinón-Torres M, Bermúdez de Castro JM. The fossil teeth of the Peking Man. *Sci. Rep.* **2018**, *8*, 2066.
40. Braga J, Zimmer V, Dumoncel J, Samir C, De Beer F, Zanolli C, et al. Efficacy of diffeomorphic surface matching and 3D geometric morphometrics for taxonomic discrimination of Early Pleistocene hominin mandibular molars. *J. Hum. Evol.* **2019**, *130*, 21–35.
41. Zanolli C, Kullmer O, Kelley J, Bacon AM, Demeter F, Dumoncel J, et al. Evidence for increased hominid diversity in the Early to Middle Pleistocene of Indonesia. *Nat. Ecol. Evol.* **2019**, *3*, 755–764.
42. Ortiz A, Bailey SE, Delgado M, Zanolli C, Demeter F, Bacon AM, et al. A distinguishing feature of Pongo upper molars and its implications for the taxonomic identification of isolated hominid teeth from the Pleistocene of Asia. *Am. J. Phys. Anthropol.* **2019**, *170*, 595–612.
43. Modesto-Mata M, Dean MC, Lacruz RS, Bromage TG, García-Campos C, Martínez de Pinillos M, et al. Short and long period growth markers of enamel formation distinguish European Pleistocene hominins. *Sci. Rep.* **2020**, *10*, 4665.
44. de Castro JM, Xing S, Liu W, García-Campos C, Martín-Francés L, de Pinillos MM, et al. Comparative dental study between Homo antecessor and Chinese Homo erectus: Nonmetric features and geometric morphometrics. *J. Hum. Evol.* **2021**, *161*, 103087.
45. Zanolli C, Davies TW, Joannes-Boyau R, Beaudet A, Bruxelles L, de Beer F, et al. Dental data challenge the ubiquitous presence of Homo in the Cradle of Humankind. *Proc. Natl. Acad. Sci. USA* **2022**, *119*, e2111212119.
46. Pan L, Zanolli C, Martinón-Torres M, de Castro JM, Martín-Francés L, Xing S, et al. Early Pleistocene hominin teeth from Gongwangling of Lantian, Central China. *J. Hum. Evol.* **2022**, *168*, 103212.
47. Davies TW, Gunz P, Spoor F, Alemseged Z, Gidna A, Hublin JJ, et al. Dental morphology in Homo habilis and its implications for the evolution of early Homo. *Nat. Commun.* **2024**, *15*, 286.
48. Luyer ML, Coquerelle M, Rottier S, Bayle P. Internal Tooth Structure and Burial Practices: Insights into the Neolithic Necropolis of Gurgy (France, 5100-4000 cal. BC). *PLoS ONE* **2016**, *11*, e0159688.
49. Le Luyer M, Coquerelle M, Rottier S, Bayle P. 3D models related to the publication: Internal tooth structure and burial practices: Insights into the Neolithic necropolis of Gurgy (France, 5100-4000 cal. BC). *M3* **2016**, *2*, 1. doi:10.18563/m3.2.1.e1.
50. R Core Team. *R: A Language and Environment for Statistical Computing*; R Foundation for Statistical Computing: Vienna, Austria, 2021.
51. Schlager S. Chapter 9—Morpho and Rvcg—Shape Analysis in R: R-Packages for Geometric Morphometrics, Shape Analysis and Surface Manipulations. In *Statistical Shape and Deformation Analysis*; Zheng G, Li S, Székely G, Eds.; Academic Press: Cambridge, MA, USA, 2017; pp. 217–256. doi:10.1016/B978-0-12-810493-4.00011-0.
52. Bookstein FL. Landmark methods for forms without landmarks: Morphometrics of group differences in outline shape. *Med. Image Anal.* **1997**, *1*, 225–243.
53. Zelditch M, Swiderski D, Sheets D. *Geometric Morphometrics for Biologists. A Primer*, 2nd ed.; Elsevier Academic Press: London, UK, 2012.
54. Dryden IL, Mardia KV. *Statistical Shape Analysis*; Wiley: Chichester, UK, 1998.
55. Dray S, Dufour A-B. The ade4 Package: Implementing the Duality Diagram for Ecologists. *J. Stat. Softw.* **2007**, *22*, 1–20.
56. Baken EK, Collyer ML, Kaliontzopoulou A, Adams DC. geomorph v4.0 and gmShiny: Enhanced analytics and a new graphical interface for a comprehensive morphometric experience. *Methods Ecol. Evol.* **2021**, *12*, 2355–2363.
57. Murdoch D, Adler D, Nenadic O, Urbanek S, Chen M, Gebhardt A, et al. rgl: 3D Visualization Using OpenGL. *R Package Version 0.108* **2021**, *3*, 443.
58. Wickham H. *Ggplot2: Elegant Graphics for Data Analysis*; Springer-Verlag: New York, NY, USA, 2016.
59. Ortiz A, Bailey SE, Hublin J-J, Skinner MM. Homology, homoplasy and cusp variability at the enamel–dentine junction of hominoid molars. *J. Anat.* **2017**, *231*, 585–599.
60. Bailey SE, Lynch JM. Diagnostic differences in mandibular P4 shape between Neandertals and anatomically modern humans. *Am. J. Phys. Anthropol.* **2005**, *126*, 268–277.
61. Gómez-Robles A, Martinón-Torres M, De Castro JB, Margvelashvili A, Bastir M, Arsuaga JL, et al. A geometric morphometric analysis of hominin upper first molar shape. *J. Hum. Evol.* **2007**, *53*, 272–285.
62. Martín-Francés L, de Castro JM, de Pinillos MM, Martinón-Torres M, Arsuaga JL, Bertrand B, et al. Middle Pleistocene hominin teeth from Biache-Saint-Vaast, France. *Archaeol. Anthr. Sci.* **2022**, *14*, 215.

63. Bailey S. Beyond Shovel-Shaped Incisors: Neandertal Dental Morphology in a Comparative Context. *Period. Biol.* **2006**, *108*, 253–267.
64. Martín-Francés L, Martinón-Torres M, Martínez de Pinillos M, García-Campos C, Zanolli C, Bayle P, et al. Crown tissue proportions and enamel thickness distribution in the Middle Pleistocene hominin molars from Sima de los Huesos (SH) population (Atapuerca, Spain). *PLoS ONE* **2020**, *15*, e0233281.
65. Benazzi S, Bailey SE, Mallegni F. Brief communication: A morphometric analysis of the neandertal upper second molar leuca I. *Am. J. Phys. Anthropol.* **2013**, *152*, 300–305.
66. Zubova AV, Moiseyev VG, Kulkov AM, Otcherednoy AK, Markin SV, Kolobova KA. Maxillary second molar from the Rozhok I Micoquian site (Azov Sea region): Another link between Eastern Europe and Siberia. *J. Hum. Evol.* **2022**, *168*, 103209.
67. Ortiz A, Skinner MM, Bailey SE, Hublin J-J. Carabelli's trait revisited: An examination of mesiolingual features at the enamel–dentine junction and enamel surface of Pan and Homo sapiens upper molars. *J. Hum. Evol.* **2012**, *63*, 586–596.
68. Martínez de Pinillos M, Martinón-Torres M, Martín-Francés L, Arsuaga JL, Bermúdez de Castro JM. Comparative analysis of the trigonid crests patterns in Homo antecessor molars at the enamel and dentine surfaces. *Quat. Int.* **2017**, *433*, 189–198.
69. Davies TW, Alemseged Z, Gidna A, Hublin JJ, Kimbel WH, Kullmer O, et al. Accessory cusp expression at the enamel-dentine junction of hominin mandibular molars. *PeerJ* **2021**, *9*, e11415.
70. Scott GR, Turner CG. *The Anthropology of Modern Human Teeth: Dental Morphology and Its Variation in Recent Human Populations*; Cambridge University Press: Cambridge, UK, 1997. doi:10.1017/CBO9781316529843.
71. Scott GR, Irish JD. *Human Tooth Crown and Root Morphology: The Arizona State University Dental Anthropology System*; Cambridge University Press: Cambridge, UK, 2017. doi:10.1017/9781316156629.
72. Ortiz A, Bailey SE, Schwartz GT, Hublin J-J, Skinner MM. Evo-devo models of tooth development and the origin of hominoid molar diversity. *Sci. Adv.* **2018**, *4*, eaar2334.
73. Bermúdez de Castro JM, Rosas A, Nicolás ME. Dental remains from Atapuerca-TD6 (Gran Dolina site, Burgos, Spain). *J. Hum. Evol.* **1999**, *37*, 523–566.
74. Smith TM, Olejniczak AJ, Zermeno JP, Tafforeau P, Skinner MM, Hoffmann A, et al. Variation in enamel thickness within the genus Homo. *J. Hum. Evol.* **2012**, *62*, 395–411.
75. Gómez-Robles A. Dental evolutionary rates and its implications for the Neanderthal–modern human divergence. *Sci. Adv.* **2019**, *5*, eaaw1268.